Performance and Reliability of Bonded Interfaces for High-temperature Packaging

Annual Progress Report

Douglas DeVoto

NREL is a national laboratory of the U.S. Department of Energy
Office of Energy Efficiency & Renewable Energy
Operated by the Alliance for Sustainable Energy, LLC

This report is available at no cost from the National Renewable Energy Laboratory (NREL) at www.nrel.gov/publications.

Management Report
NREL/MP-5400-67117
October 2017

Contract No. DE-AC36-08GO28308

NREL
NATIONAL RENEWABLE ENERGY LABORATORY

Performance and Reliability of Bonded Interfaces for High-temperature Packaging

Annual Progress Report

Douglas DeVoto

NREL is a national laboratory of the U.S. Department of Energy
Office of Energy Efficiency & Renewable Energy
Operated by the Alliance for Sustainable Energy, LLC

This report is available at no cost from the National Renewable Energy Laboratory (NREL) at www.nrel.gov/publications.

National Renewable Energy Laboratory
15013 Denver West Parkway
Golden, CO 80401
303-275-3000 • www.nrel.gov

Management Report
NREL/MP-5400-67117
October 2017

Contract No. DE-AC36-08GO28308

Cover Photos by Dennis Schroeder: (left to right) NREL 26173, NREL 18302, NREL 19758, NREL 29642, NREL 19795.

NREL prints on paper that contains recycled content.

Performance and Reliability of Bonded Interfaces for High-Temperature Packaging

Principal Investigator: Douglas DeVoto
National Renewable Energy Laboratory (NREL)
15013 Denver West Parkway
Golden, CO 80401
Phone: 303-275-4256
Email: douglas.devoto@nrel.gov

DOE Technology Development Manager: Susan A. Rogers
U.S. Department of Energy
1000 Independence Ave. SW EE-3V
Washington, DC 20585
Phone: 202-586-8997
Email: susan.rogers@ee.doe.gov

NREL Task Leader: Sreekant Narumanchi
Phone: 303-275-4062
Email: sreekant.narumanchi@nrel.gov

Abstract/Executive Summary

Current generation automotive power electronics packages utilize silicon devices and lead-free solder alloys. To meet stringent technical targets for 2020 and beyond (for cost, power density, specific power, efficiency, and reliability), wide-bandgap devices are being considered because they offer advantages such as operation at higher frequencies, voltages, and temperatures. Traditional power electronics packages must be redesigned to utilize the full potential of wide-bandgap devices, and the die- and substrate-attach layers are key areas where new material development and validation is required. Present solder alloys do not meet the performance requirements for these new package designs while also meeting cost and hazardous substance restrictions.

Sintered silver (Ag) promises to meet the needs for die- and substrate-attach interfaces but synthesis optimization and reliability evaluations must be completed. Sintered Ag material was proposed as an alternative solution in power electronics packages almost 20 years ago. However, synthesis pressure requirements up to 40 MPa caused a higher complexity in the production process and more stringent flatness specifications for the substrates. Recently, several manufacturers have developed sintered Ag materials that require lower (3–5 MPa) or even no bonding pressures.

Degradation mechanisms for these sintered Ag materials are not well known and need to be addressed. We are addressing these aspects to some extent in this project. We are developing generalized (i.e., independent of geometry) J-Integral versus cycles-to-failure relations for sintered Ag. Because sintered Ag is a relatively new material for automotive power electronics, the industry currently does not have a good understanding of recommended synthesis parameters or expected reliability under prescribed conditions. It is an important deliverable of this project to transfer findings to industry to eliminate barriers to using sintered Ag as a viable and commercialized die- and substrate-attach material. Only a few manufacturers produce sintered Ag pastes and may consider some processing conditions as proprietary. It is the goal of this project to openly explore and define best practices in order to impact the maximum number of power electronics module manufacturers and suppliers.

Accomplishments

- Modeled strain energy density and J-Integral values for sintered coupons with round and 50-mm x 50-mm geometries under thermal cycling conditions.

- Synthesized and shear tested initial samples for mechanical characterization of sintered Ag. Material properties gathered are replacing bulk silver material properties to more accurately model the interface structure.

✧ ✧ ✧ ✧ ✧

Introduction

Standard packaging technologies have limited the advancement of automotive power electronics modules toward designs that promise higher performance and reliability. The drive toward reduced cost, weight, and volume of components in electric-drive vehicles has led to increased performance demands on power electronics modules. Increased power densities and larger temperature extremes reduce lifetimes for traditional power electronics packages and require new materials and manufacturing processes to be utilized. Before new technologies can be introduced into commercial products, their reliability must be evaluated and quantified.

Current power electronics packages utilize silicon devices and lead-free solder alloys within their construction. As package designs transition to wide-bandgap devices, interface materials must improve to fully utilize the capabilities of these new devices [1-6]. Current solder alloys exhibit creep effects when subjected to elevated temperatures and cannot operate at temperatures as high as 200°C. The operating ranges of several currently used interface materials are shown in Figure 1.

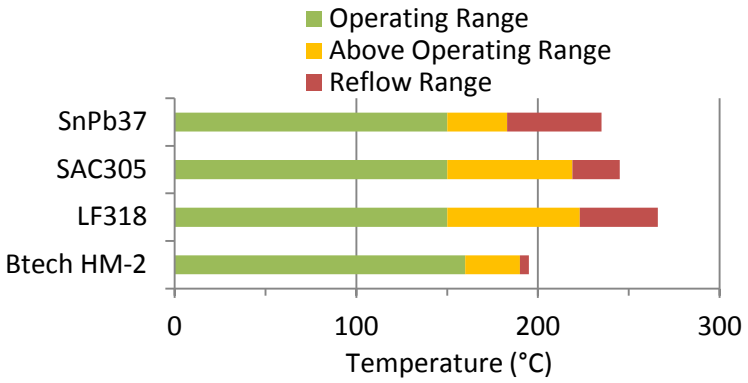

Figure 1: Operating range of common interface materials

Research efforts for high-temperature bonded interface materials can be roughly classified into three categories: Ag sintering, high-temperature soldering, and transient liquid phase (TLP) sintering. The advantages and disadvantages to these processing technologies are summarized in Table 1.

Table 1: Emerging die- and substrate-attach processes

Process	Advantages	Disadvantages
Ag sintering	High thermal conductivity, highest operating temperature	High processing pressure, material cost
High-temperature soldering	Similar to current soldering procedures	High processing temperature, higher residual stresses, material cost
TLP sintering	Minimal bonding pressure	Processing time, navigating phase diagrams

Some solder alloys have been developed for high-temperature operation, but face cost limitations (e.g., gold alloys) or do not meet Restriction of Hazardous Substances standards (e.g., high-lead alloys). Additionally, solder alloys must always be processed at temperatures higher than their desired operating temperature because their reflow temperatures are equivalent to their processing temperature. This imparts higher residual stresses onto the devices and insulating substrates during processing. Some power electronics module suppliers are evaluating high-temperature solders as a "drop-in" replacement to previously used solder alloys and acknowledge the higher associated material costs.

TLP sintering involves an assembly or paste of low- and high-melt materials. Processing occurs at low temperatures (250°C–300°C) where the low-melt component material diffuses into the high-melt material to form intermetallic compounds. These intermetallic compounds will only re-melt at temperatures much higher than the processing conditions (400°C–600°C). Toyota Research Institute of North America has several publications on the development of nickel-tin (Ni-Sn) TLP bonding for automotive power electronics. The University of Maryland's Center for Advanced Life Cycle Engineering is working to develop Ni-Sn and copper-tin (Cu-Sn) TLP bonding systems while Ames Laboratory has developed a Cu-Ni TLP process.

Sintered Ag material was proposed as an alternative solution in power electronics packages as far back as 20 years ago. To reduce synthesis temperatures to below 300°C, the concurrent application of pressure up to 40 MPa onto the package or sintered Ag bonded interface material was originally advocated. However, this caused a higher complexity in the production process and more stringent flatness specifications for the substrates. Recently, several manufacturers have developed sintered Ag materials that require lower (3–5 MPa) or even no bonding pressures. Virginia Tech, Heraeus, Henkel, and Kyocera have developed these materials. Semikron currently has production power electronics using sintered Ag as the die-attach layer. Large-area substrate attachment, as well as low-pressure synthesis, requires additional research and development for power electronics module suppliers to transition to sintered Ag. Prior work at NREL and Oak Ridge National Laboratory has demonstrated the promise of the processing technology, but a comprehensive evaluation of all processing variables is needed to demonstrate best practices to industry.

Approach

Finite element simulations in ANSYS were conducted to obtain the desired modeling parameters to develop a predictive lifetime model for sintered Ag. The two parameters of interest are strain energy density and J-integral. Strain energy density is calculated as the time integral of product of stresses and incremental strains at any given node, and has been identified as a suitable parameter for predictive lifetime models [7].

In the previous year, J-integral [8] was identified as the fracture mechanics parameter to be computed using finite element analysis. J-integral, a contour integral around the crack tip, is a convenient parameter for crack tip studies mainly because of its path-independent nature. However, it has to be noted that the path independence of J-integral for elastic-plastic materials holds only under certain circumstances, such as when the material behavior can be described based on deformation theory of plasticity or when the material is subjected to purely monotonic loading. Under such circumstances, elastic-plastic materials can be idealized as non-linear elastic materials and the J-integral effectively characterizes the crack tip field parameters. A few researchers have proved that the incremental theory of plasticity mimics the deformation theory of plasticity, but only when the loading is proportional. Nevertheless, under the incremental theory of plasticity, the path-dependent nature of J-integral becomes less pronounced with successive contours around a crack tip and exhibits a converging trend [9]. This converged value can be considered as a valid parameter that defines the crack tip field. The relevance of parameters computed numerically can be justified only after developing a model fit with experimental results, and determining the accuracy of that fit in predicting lifetime of sintered Ag samples tested under different loading conditions.

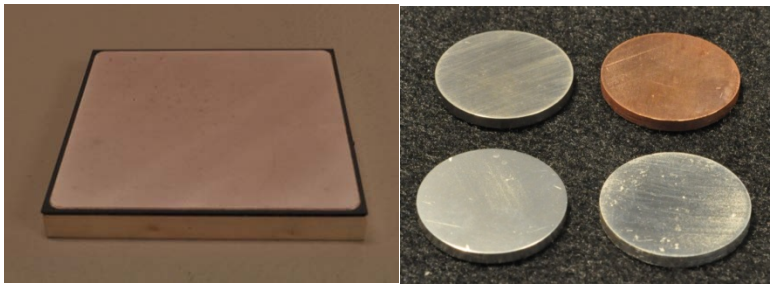

Figure 2: A) 50-mm x 50-mm sample (left), and B) copper and Invar coupons (right)

Simulations were performed on both 50-mm x 50-mm samples and round coupons shown in Figures 2A and 2B, respectively. For a given configuration, multiple simulations with decreasing bond pad areas were run to simulate crack propagation. Thermal cycle temperature loads for round coupons were -40°C and 170°C, whereas the 50-mm x 50-mm samples were subjected to a thermal cycle between -40°C and 150°C. Strain energy density results were volume-averaged over the entire circular bond pad region of round coupons to avoid singularity issues. For 50-mm x 50-mm sample simulations with crack feature inserted into the model, it was found that J-integral results converged to within 5% after six contours around the crack front.

Results and Discussion

Round Coupons

The round coupon samples were of three different types—copper-Invar, copper-copper, and Invar-Invar—all with sintered Ag as the joint. Figure 3 shows a plot of strain energy density per cycle values of copper-Invar samples with varying bond pad diameters. A red triangle dot indicates that the result corresponds to an actual sample that was tested experimentally. Reading the graph from right to left, it can be inferred that a reduction in the bond pad diameter results in higher values of strain energy density per cycle, but only up to a certain diameter. Beyond that point, strain energy density decreases slightly. For any bond pad diameter, strain energy density is more concentrated on the outer regions and decreases toward the center. Also, a detailed analysis shows that strain energy density is predominant in the out-of-plane shear planes, as shown in Figure 4.

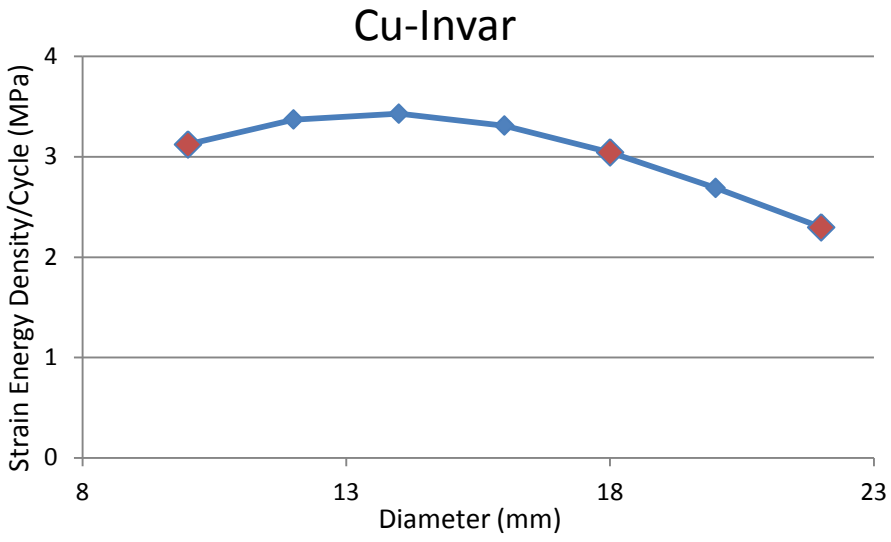

Figure 3: Strain energy density per cycle results of copper-Invar samples

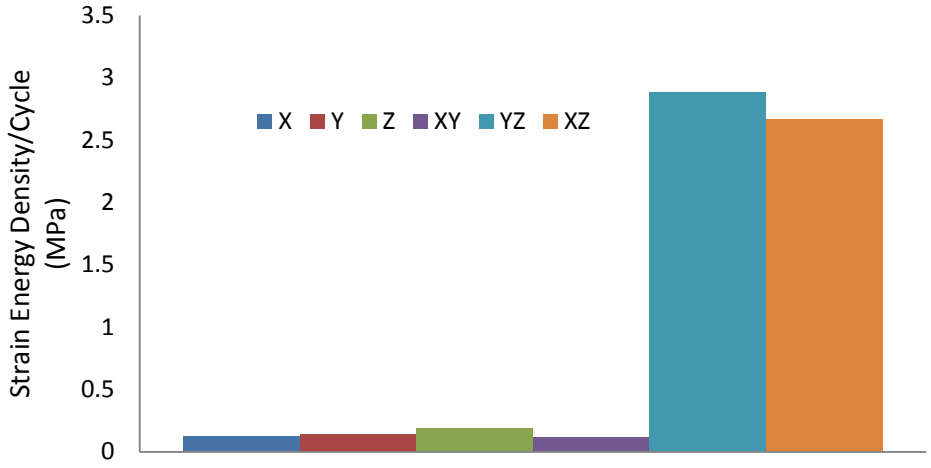

Figure 4: Strain energy density per cycle components of an element split in six directions

Figure 5 shows a plot of strain energy density per cycle values of copper-copper and Invar-Invar bonded samples with varying bond pad diameters. Although not as severe as the global coefficient of thermal expansion (CTE) mismatch between the adherend coupons, the local CTE mismatch between Invar and sintered Ag results in a higher strain energy density for Invar-Invar samples than copper-copper samples. As compared to copper-Invar samples, bond pad diameter variation does not have any impact on the strain energy density of sintered Ag due to little CTE mismatch in the out-of-plane directions. Hence, changing an in-plane dimension of the joint will not affect the strain energy density.

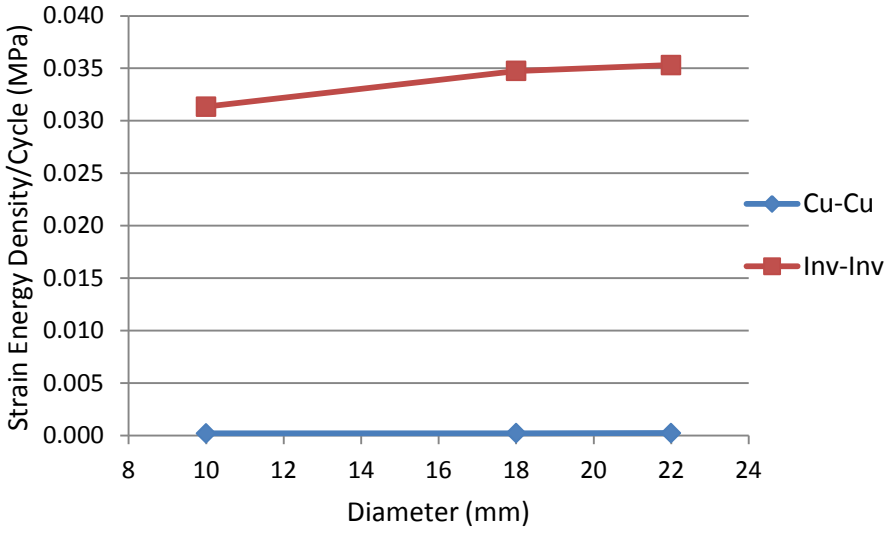

Figure 5: Strain energy density per cycle results of copper-copper and Invar-Invar samples

50-mm x 50-mm

Samples measuring 50 mm x 50 mm were also included in the modeling study as C-mode scanning acoustic microscopy images of the sintered Ag interface within the sample were already available from a previous project. A non-linear finite element method analysis showed that higher values of strain energy density occur at the corner regions of the sintered Ag joint and is where cracks are likely to initiate. A meshed model of the geometry with crack feature (not visible) inserted in the corner region is shown in Figure 6a. A higher mesh density is implemented in the corner regions around the crack front to adequately capture the effect of crack front on the stress and displacement fields. The focus was mainly on calculating the J-integral values with these samples. Six concentric contours were created around the crack front (red line) for evaluating the J-integral values as shown in Figure 6b. The Anand model was used as the material constitutive model and the

model parameters were obtained from the literature [10]. Multiple simulations with reduced bonded areas were conducted as an indirect way of simulating crack propagation, as shown in Figure 7.

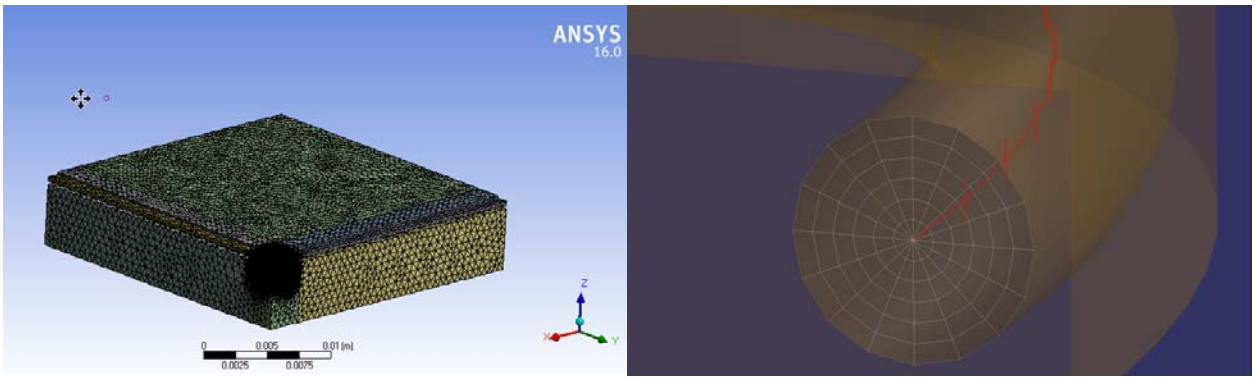

Figure 6: Quarter-symmetric model of 50-mm x 50-mm sample with a) tetrahedral mesh (left), and b) J-Integral contours shown (right)

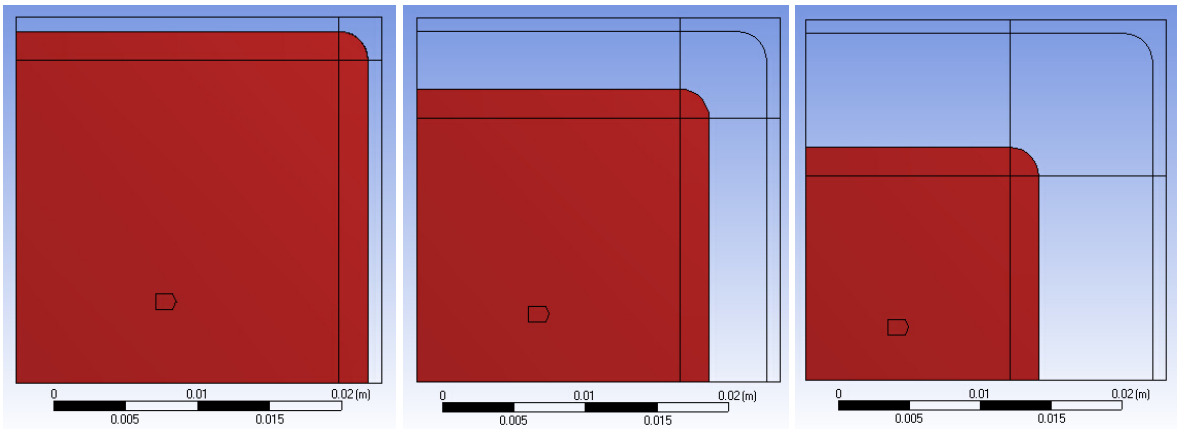

Figure 7: Samples measured 50 mm x 50 mm with reduced bonded areas shown by the red region, where joint area is a) 48.4-mm x 48.4-mm (left), b) 40.4-mm x 40.4-mm (center), and c) 32.4-mm x 32.4-mm (right)

Thermal cyclic loading was repeated for four cycles before the results converged. After solution, a contour plot of J-integral along the crack front was obtained in the post processing phase. Analysis of J-integral values at the crack front nodes from each contour show that path dependence becomes less pronounced with each successive contour and is within 5% to 6% after six contours. In order to avoid any singularity issues, J-integral values from the sixth contour were then averaged along the crack front nodes. Also, J-integral, being a cumulative value, keeps increasing with each thermal cycle. Hence, J-integral over a thermal cycle range was obtained and taken as the final output. Figure 8 shows a plot of J-integral along the crack front.

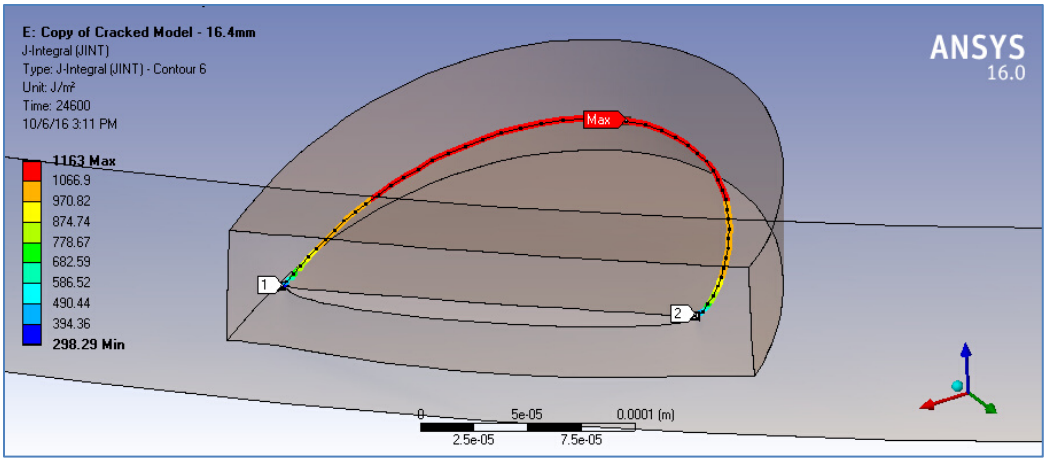

Figure 8: J-integral plot

The obtained values of the J-integral along the crack contour are compiled in Table 2.

Table 2: J-integral/cycle for 50-mm x 50-mm samples

Bond Pad Area	J-Integral/Cycle (J/m^2)
48.4 x 48.4	114.1
40.4 x 40.4	188.7
32.4 x 32.4	222.2

Strain energy density per cycle results were also calculated for the 50-mm x 50-mm samples. Simulations were performed without the crack feature for different bond areas, and strain energy density results were volume-averaged over the corner fillet region. These results are plotted in Figure 9, shown below.

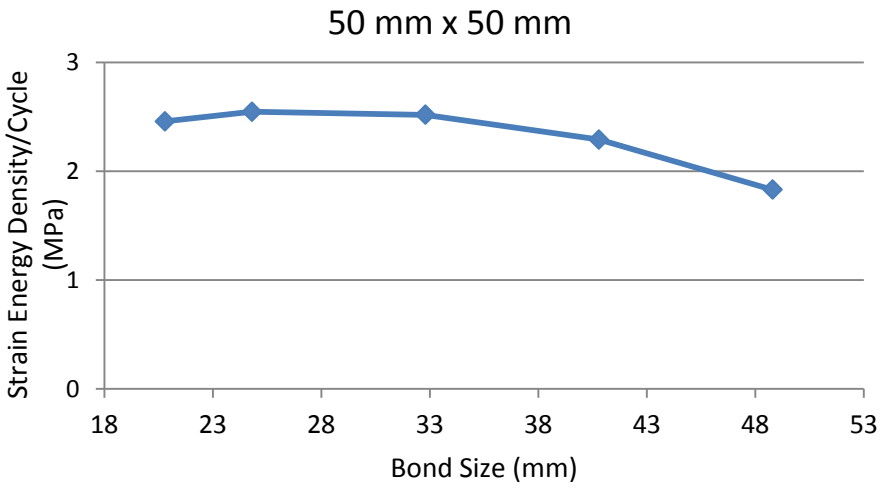

Figure 9: Strain energy density results for 50-mm x 50-mm samples

Mechanical Testing

Prior testing found that poor bonding of the Cu-Invar round samples due to the intended CTE mismatch quickly led to separation of the test coupons [6]. This was consistently shown for 10-, 18-, and 22-mm bond pad diameter samples, with no samples reaching 500 cycles. Several Invar-Invar samples also failed, with two of the three failures occurring in the samples that were sintered for a longer duration. New samples were sintered for shear testing in the hopes that improved shear strength will lead to stronger round coupons. While the mechanical properties of bulk Ag are well known, variations in paste manufacture, drying procedure, and sintering method can all lead to significant differences in properties for sintered Ag. To obtain the needed material properties for accurate modeling of the interface, shear testing of the material was completed. Three Cu coupons comprise the shear test sample, all 12.7-mm x 12.7-mm square. The middle coupon is 5-mm thick while the outer coupons are 1.8-mm thick. The desired bonded interface material is used to adhere the three coupons together into a test sample. This sample is placed in a shear test fixture that supports the outer coupons while applying a load to the middle coupon. The symmetry of the test samples allows for the interface layers to be loaded in a pure shear fashion. A test sample and the shear fixture are shown in Figure 10. The shear fixture is placed within an Instron 5966 dual column testing system that can be configured with 100 N and 10 kN load cells. The environmental chamber has a temperature range from -100°C to 350°C for capturing temperature-dependent material properties. A noncontact video extensometer is used for strain measurements. The Instron mechanical testing system is shown in Figure 10.

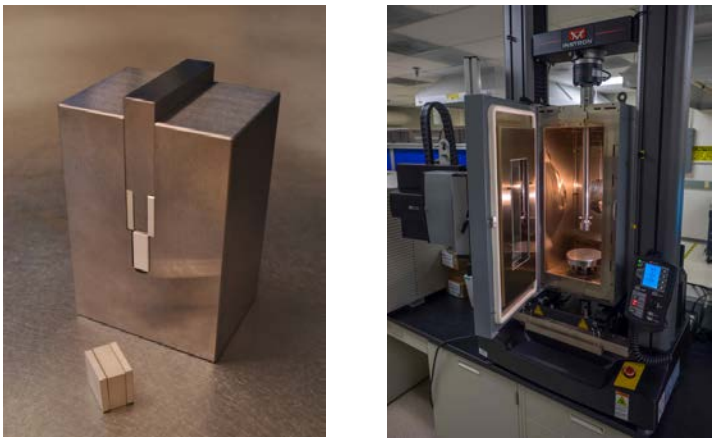

Figure 10: Test sample and shear test fixture (left) and Instron mechanical testing system (right)

To validate the shear testing procedure, $Sn_{63}Pb_{37}$ solder was used to synthesize several samples. Solder preforms were placed between the test coupons along with a few glass beads to ensure planarity of the bond line. After a solder reflow process was completed, the bond layers were inspected by acoustic microscopy. Only samples with minimal voiding were selected for shear testing. After screening, samples were placed within the shear test fixture and sheared at a strain rate of 0.02. The video extensometer measured displacement change of the fixture and the testing system recorded the compressive loading. Shear stress was calculated by dividing the compressive loading force by the bonded area of the test coupons. The acoustic images revised the bonded area by subtracting voided areas. A compilation of stress-strain curves of five $Sn_{63}Pb_{37}$ solder samples is shown in Figure 11.

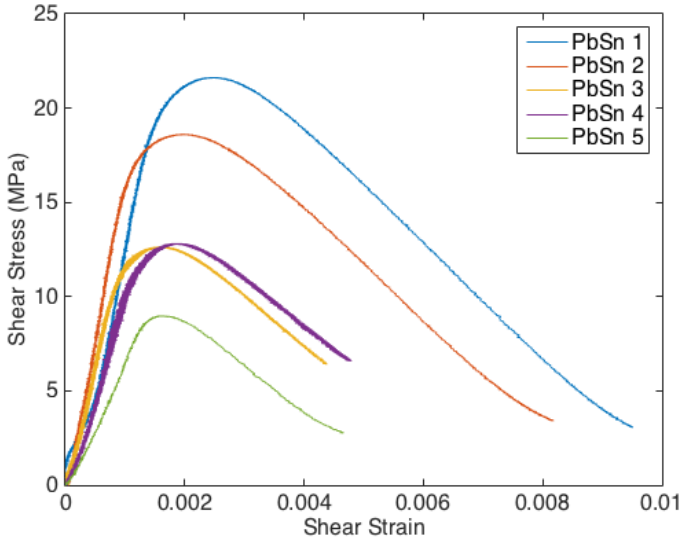

Figure 11: Solder stress-strain curves

Maximum shear stress values varied among samples between eight and 22 MPa. Shear testing was repeated with sintered Ag samples. Stress-strain curves of eight samples are shown in Figure 12.

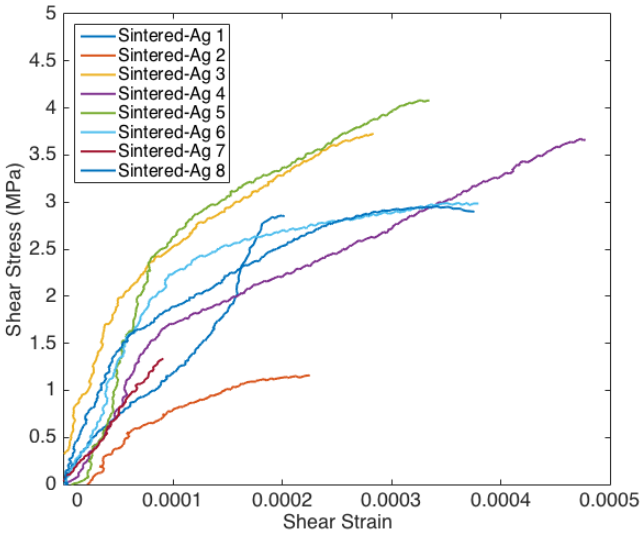

Figure 12: Sintered Ag stress-strain curves

When compared to the $Sn_{63}Pb_{37}$ solder samples, it was found that sintered Ag samples reached their ultimate strength with very little displacement, confirming that creep effects are minimal within the material. Variation in ultimate strength varied more from sample to sample and may be due to the synthesis variations between samples. The maximum shear stress values for sintered Ag are also significantly lower than measurements of $Sn_{63}Pb_{37}$ solder samples, indicating that additional synthesis optimization for sintered Ag is required.

Conclusions and Future Directions

As maximum device temperatures approach 200°C continuous operation, sintered Ag materials promise to maintain bonds at these high temperatures without excessive degradation rates. Recent work has modeled strain energy density and J-Integral values for sintered coupons with round and 50-mm x 50-mm geometries under thermal cycling conditions. Sintered Ag samples were synthesized and shear tested for mechanical characterization. Material properties gathered are replacing bulk silver material properties to more accurately model the interface structure. Working in close collaboration with Kyocera and Virginia Tech, a detailed

characterization of the thermal performance and reliability of sintered Ag materials and processes has been initiated for the next year.

Future steps in crack modeling include efforts to simulate crack propagation directly using the extended finite element method (X-FEM). X-FEM is a numerical technique that uses partition of unity method for modeling discontinuities such as cracks in a system. The biggest advantage of X-FEM is that crack propagation can be modeled without re-meshing. Also, we will investigate the application of cohesive zone models, which employ traction-separation laws, in an X-FEM framework to simulate cohesive crack growth.

Development of lifetime estimation tools will allow the reliability of sintered Ag to be predicted (similar to the reliability prediction of solder materials), and enable a time- and cost-effective design process. Performance and reliability of novel/emerging techniques such as atomic-level bonding (in collaboration with industry) will also be investigated as a longer-term development goal.

FY 2016 Presentations/ Publications/ Patents

1. P. Paret, D. DeVoto, and S. Narumanchi. 2016. "Reliability of Emerging Bonded Interface Materials for Large-Area Attachments." *IEEE Transactions on Components, Packaging and Manufacturing Technology* Vol. 6, No. 1, pp. 40-49.
2. A.A. Wereszczak, M.C. Modugno, S.B. Waters, D.J. DeVoto, and P.P. Paret. 2016. "Method to Determine Maximum Allowable Sinterable Silver Interconnect Size." IMAPS High Temperature Electronics (HiTEC), Albuquerque, NM.

Acknowledgments

The author would like to acknowledge the support provided by Susan Rogers, Technology Development Manager for the Electric Drive Technologies Program, Vehicle Technologies Office, U.S. Department of Energy Office of Energy Efficiency and Renewable Energy. The significant contributions of Andrew Wereszczak, Paul Paret, Jake Callaghan, Meghan Herbert-Walters, and Joshua Major are acknowledged.

References

1. A.A. Wereszczak, Z. Liang, M.K. Ferber, and L.D. Marlino. 2014. "Uniqueness and Challenges of Sintered Silver as a Bonded Interface Material." International Conference on High Temperature Electronics (HiTEC), Albuquerque, NM.
2. R.W. Chuang and C.C. Lee. 2002. "Silver-Indium Joints Produced at Low Temperature for High Temperature Devices." *IEEE Transactions on Components and Packaging Technologies* Vol. 25, No. 3, pp. 453–458.
3. K. Sow. 2014. "Are Sintered Silver Joints Ready for Use as Interconnect Material in Microelectronic Packaging?" *Journal of Electronic Materials* Vol. 43, No. 4, pp. 947–961.
4. S.W. Yoon, K. Shiozaki, S. Yasuda, and M.D. Glover. 2012. "Highly Reliable Nickel-Tin Transient Liquid Phase Bonding Technology for High Temperature Operational Power Electronics in Electrified Vehicles." Twenty-Seventh Annual IEEE Applied Power Electronics Conference and Exposition (APEC), pp. 478–482.
5. H. Greve and F.P. McCluskey. 2014. "LT-TLPS Die." *Journal of Microelectronics and Electronic Packaging* Vol. 11, No. 1, pp. 7–15.
6. D.J. DeVoto, A.A. Wereszczak, and P.P. Paret. 2014. "Stress Intensity of Delamination in a Sintered-Silver Interconnection." IMAPS High Temperature Electronics (HiTEC), Albuquerque, NM.
7. P. Paret, D. DeVoto, and S. Narumanchi. 2016. "Reliability of Emerging Bonded Interface Materials for Large-Area Attachments." IEEE Transactions on Components, Packaging and Manufacturing Technology, Vol. 6, No. 1, pp. 40–49.
8. J.R. Rice. 1968. "A Path Independent Integral and Approximate Analysis of Strain Concentration by Notches and Cracks." ASME Journal of Applied Mechanics, Vol. 35, pp. 379–386.

9. W. Brocks and I. Scheider. 2001. “Numerical Aspects of the Path-Dependence of the J-Integral in Incremental Plasticity.” Technical Note GKSS/WMS/01/08.
10. X. Chen, R. Li, K. Qi, and G.Q. Lu. 2008. “Tensile behaviors and Ratcheting Effects of Partially Sintered Chip-Attachment Films of a Nanoscale Silver Paste.” *Journal of Electronic Materials* Vol. 37, No. 10.